Deterministic generation of remote entanglement with active quantum feedback

Leigh Martin,[1,2,*] Felix Motzoi,[1,2,3,†] Hanhan Li,[1,2] Mohan Sarovar,[4] and K. Birgitta Whaley[1,3]
[1]*Berkeley Center for Quantum Information and Computation, Berkeley, California 94720, USA*
[2]*Department of Physics, University of California, Berkeley, Berkeley, California 94720, USA*
[3]*Department of Chemistry, University of California, Berkeley, Berkeley, California 94720, USA*
[4]*Digital & Quantum Information Systems, Sandia National Laboratories, Livermore, California 94550, USA*
(Received 10 July 2015; published 10 December 2015)

We consider the task of deterministically entangling two remote qubits using joint measurement and feedback, but no directly entangling Hamiltonian. In order to formulate the most effective experimentally feasible protocol, we introduce the notion of average-sense locally optimal feedback protocols, which do not require real-time quantum state estimation, a difficult component of real-time quantum feedback control. We use this notion of optimality to construct two protocols that can deterministically create maximal entanglement: a semiclassical feedback protocol for low-efficiency measurements and a quantum feedback protocol for high-efficiency measurements. The latter reduces to direct feedback in the continuous-time limit, whose dynamics can be modeled by a Wiseman-Milburn feedback master equation, which yields an analytic solution in the limit of unit measurement efficiency. Our formalism can smoothly interpolate between continuous-time and discrete-time descriptions of feedback dynamics and we exploit this feature to derive a superior hybrid protocol for arbitrary nonunit measurement efficiency that switches between quantum and semiclassical protocols. Finally, we show using simulations incorporating experimental imperfections that deterministic entanglement of remote superconducting qubits may be achieved with current technology using the continuous-time feedback protocol alone.

DOI: 10.1103/PhysRevA.92.062321 PACS number(s): 03.67.Bg

I. INTRODUCTION

Engineering of quantum devices requires optimization of two essentially contradictory requirements. On the one hand, quantum properties such as superposition and entanglement upon which these devices rely are fragile and require careful isolation from external degrees of freedom. On the other hand, control and measurement of a system requires coupling to an external device, which often runs contrary to the necessity for decoupling from the environment. To balance this trade-off, many quantum systems relevant for quantum computing and sensing lack readout capabilities that are effectively instantaneous and projective. Instead, measurement occurs over a finite resolvable time scale in such systems. Recent research has taken advantage of this by utilizing the fact that continuous weak measurement enables direct observation of the continuous-time evolution of a quantum system (quantum trajectories) [1–4] and also permits operations on the system *during* the measurement process, including feedback and feedforward control [5–8].

Real-time quantum feedback control is expected to be broadly applicable to many problems in quantum information science. Some quantum information applications that have been proposed to date include rapid purification of qubits or qubit registers [9–14], quantum error correction [15,16], transmission of quantum information through noisy channels [17], adaptive measurement for quantum state discrimination [18–20], and several forms of quantum state preparation and stabilization [21–25].

Experimentally, quantum feedback has been mostly demonstrated to date with atomic, molecular, or optical systems (see, e.g., [6,7]). However, the advent of quantum-limited microwave amplifiers has recently enabled experimental realization of quantum feedback in superconducting circuits, where it has been used to stabilize the Rabi oscillations of a single qubit [8] and to deterministically create entanglement of two qubits within a single cavity [26] using a discrete feedback loop.

Several works have also suggested using quantum feedback to enhance generation of remote entanglement [27–30]. These papers have considered the case in which the controller has access to a joint measurement on a pair of qubits that are too far apart to engineer a direct or photon-mediated interaction, an important scenario for quantum networks or large-scale quantum computers [31]. The remote aspect requires that the quantum feedback operations be restricted to local unitaries, which cannot on their own generate entanglement [32]. Conversely, a joint measurement alone cannot deterministically project a separable system into a fixed entangled state, but access to this measurement and local unitary feedback can [33].

In this work we build upon this literature in our goal to achieve optimal protocols for remote entanglement, focusing in particular on joint measurements that have been implemented in superconducting qubits [4]. We motivate our approach by an examination of optimality for the state update in a single discrete-time step and define an average-sense locally optimal (ASLO) strategy that makes the state update over this discrete-time step using the most recent measurement outcome and knowledge of the average state. We show that this discrete-time step protocol reduces to a direct feedback protocol in the continuous-time limit, whose dynamics can be modeled by a Wiseman-Milburn feedback master equation with an analytic solution that yields a simple closed-form

*Leigh@Berkeley.edu
†Current address: Theoretical Physics, Saarland University, 66123 Saarbrücken, Germany.

expression for the locally optimal quantum feedback in this limit. This analytic solution shows that for unit measurement efficiency, the fidelity with respect to the target entangled state asymptotically approaches exponentially 1. The discrete-time step optimality study also motivates a semiclassical protocol that is more effective for low measurement efficiencies, provided one takes longer time steps between applications of feedback. This feedback strategy is capable of fully entangling the qubits even for nonunit efficiency, but creates entanglement more slowly than the continuous case. Both semiclassical and quantum protocols asymptotically approach unit entanglement fidelity under unit measurement efficiency. In the case of nonideal measurements, the preferred form of the optimal feedback protocol is found to depend on the measurement efficiency η, with the semiclassical (quantum) protocol being preferred for low- (high-) η values. We then show that for arbitrary nonunit efficiency, continuously tuning the measurement time leads to a protocol that can surpass this ASLO strategy and switches from using the quantum protocol at short times to the semiclassical protocol at larger times.

The remainder of the paper is organized as follows. In Sec. II we describe the measurement that conditions our feedback using both stochastic master equation and positive-operator-valued measure (POVM) descriptions. Section III derives the optimal feedback unitary for a single discrete-time step as a function of the prior state of the qubits. We first consider the case of inefficient measurement in Sec. IV, where we neglect coherence terms of the density matrix that are dephased by the measurement to obtain a semiclassical strategy. In Sec. V we use the full density matrix for the system to derive a quantum strategy that is valid in the continuous measurement limit. In Sec. VI we combine the semiclassical and quantum protocols to develop a superior hybrid protocol that allows unit fidelity to be reached for arbitrary nonunit measurement efficiencies. Section VII demonstrates the experimental feasibility of the continuous-time ASLO protocol with numerical simulations of remote entanglement generation in a realizable system of transmon qubits in spatially separated cavities. Section VIII summarizes and provides an outlook for future work.

II. ENTANGLEMENT VIA MEASUREMENT

To study feedback in the context of remote entanglement generation, we must first describe the measurement on which the feedback will rely. As analyzed in [34], it is possible using a dispersive homodyne readout to implement a half-parity measurement in the superconducting circuit architecture. In Ref. [4], the authors succeeded in applying this measurement to two superconducting transmon qubits separated by over a meter. Reference [35] describes another scheme for implementing the required measurement, also in circuit QED. This measurement is characterized by the operator

$$X = \tfrac{1}{2}(\sigma_{z1} + \sigma_{z2}), \tag{1}$$

where σ_{zi} is the Pauli operator acting on the ith qubit. This can be used to probabilistically generate entanglement by first preparing the separable uniform superposition state $|\psi_0\rangle = \frac{1}{2}(|00\rangle + |01\rangle + |10\rangle + |11\rangle)$ (e.g., by making two local σ_y rotations on the ground state $|11\rangle$) and then measuring X. Since this observable cannot distinguish the states $|01\rangle$ and $|10\rangle$, such a measurement (if perfect) will with 50% probability project the initially unentangled $|\psi_0\rangle$ into the entangled triplet state $|t0\rangle = \frac{1}{\sqrt{2}}(|01\rangle + |10\rangle)$.

In the superconducting qubit architecture, the implementation of the measurement is such that projection onto one of the eigenstates of X can be said to occur only after a resolvable time period. During this time interval one can then perform feedback on the system based on information already gained. The measured value of the observable X is obtained from a homodyne measurement of the voltage V [4]. During the measurement, the time-dependent homodyne voltage that constitutes the measurement signal is specified by [36]

$$dV_t = \langle X\rangle(t)dt + \frac{dW(t)}{\sqrt{8\eta k}}, \tag{2}$$

where $\langle\cdot\rangle$ denotes an expectation value under $\rho(t)$, the state of the two-qubit system, k is the strength of the measurement, $0 \leqslant \eta \leqslant 1$ is the measurement efficiency, and $dW(t)$ is a Wiener increment satisfying $dW(t)dW(t') = \delta(t-t')dt$ that represents the quantum noise in the homodyne detection [5]. Note that we have chosen dV to have units of time, so the average signal $\Delta V = \frac{1}{\Delta t}\int dV$ is unitless. Experimentally, the appropriate scale factor can be extracted simply by preparing states with $\langle X\rangle = \{1, 0, -1\}$ and measuring $\langle \Delta V\rangle$ for any pair of these states.

The state of the system conditioned on this continuous measurement record is given by the following stochastic master equation [5]:

$$\rho_{dV}(t+dt) = \rho(t) + \mathcal{D}[M]\rho(t)dt + \mathcal{H}[M]\rho(t)\sqrt{\eta}dW(t),$$
$$M \equiv \sqrt{2k}X, \tag{3}$$

Here $\mathcal{D}[M] \equiv M\rho M^\dagger - 1/2(M^\dagger M\rho + \rho M^\dagger M)$ and $\mathcal{H}[M]\rho \equiv M\rho + \rho M^\dagger - \langle M + M^\dagger\rangle\rho$ (throughout this paper we use units such that $\hbar = 1$). The second term in Eq. (3) represents the dephasing due to the measurement and the third term represents the information update of the system state derived from the measurement outcome. Note that Eq. (3) is expressed in the interaction picture with respect to the free Hamiltonian for the two-qubit system $H_0 = -\frac{\omega_1}{2}\sigma_{z1} - \frac{\omega_2}{2}\sigma_{z2}$.

Equation (3) generates a set of stochastic quantum trajectory equations that provides a description of the measurement conditioned dynamics in continuous time. In the following we will also be interested in the conditioned dynamics at discrete-time intervals. In order to obtain such a discretized description of the system, we must compute the finite-time generalized measurement, or POVM [5,37] that is associated with the above continuous-time weak measurement. Such finite-time POVM descriptions are generally difficult to compute for weak measurements. However, in the case of quantum nondemolition (QND) measurements, for which $[H_0, X] = 0$, this can be readily derived. As shown in the Appendix, the finite-time POVM for such weak QND measurements is composed of a set of effects $E(\Delta V) = \Omega_{\Delta V}^\dagger\Omega_{\Delta V}$ [37], with $\Omega_{\Delta V}$ an operator corresponding to the measurement of voltage increment ΔV during a finite-time interval Δt. These effects satisfy the completion property $\int E(\Delta V)d(\Delta V) \equiv \int \Omega_{\Delta V}^\dagger\Omega_{\Delta V}d(\Delta V) = \mathbf{1}$, where the integral is performed over the domain of the voltage increment. As shown in the Appendix, in the case of perfect measurement efficiency $\eta = 1$, the operator corresponding to

the above weak measurement is given by

$$\Omega_{\Delta V} = \left(\frac{4k\Delta t}{\pi}\right)^{1/4} \exp[-2k\Delta t(\Delta V - X)^2]. \quad (4)$$

The state update corresponding to a discrete-time measurement outcome ΔV is then given by the familiar relation $\rho \to \Omega_{\Delta V}\rho\Omega_{\Delta V}^\dagger/\mathrm{Tr}[\Omega_{\Delta V}\rho\Omega_{\Delta V}^\dagger]$. In order to model inefficient measurement, we note that a weak QND measurement with strength k and efficiency $\eta \neq 1$ can be viewed as a sequence of two weak measurements of the same observable, the first with strength $k\eta$ and the second with strength $k(1-\eta)$, where we integrate out the latter in order to model the loss of this portion of the measurement signal. The measurement operator corresponding to the observed fraction η of the signal is given by

$$\Omega_{\Delta V,\eta} = \left(\frac{4\eta k\Delta t}{\pi}\right)^{1/4} \exp[-2\eta k\Delta t(\Delta V - X)^2]. \quad (5)$$

After evolution by Eq. (3) for a discrete time Δt, the two-qubit state conditioned on the finite voltage increment ΔV is then given by

$$\rho_{\Delta V}(t+\Delta t) = \int_{-\infty}^{\infty} \Omega_{\Delta V',1-\eta} \frac{\Omega_{\Delta V,\eta}\rho(t)\Omega_{\Delta V,\eta}^\dagger}{\mathrm{Tr}[\Omega_{\Delta V,\eta}\rho(t)\Omega_{\Delta V,\eta}^\dagger]} \times \Omega_{\Delta V',1-\eta}^\dagger d(\Delta V'). \quad (6)$$

Equations (3) and (6) define the time evolution of ρ under generalized measurement of the observable X for continuous- and discrete-time increments, respectively. In Fig. 1 we plot histograms of the measurement outcomes for $\eta = 1$ and $\eta = 0.2$, at a fixed measurement time Δt. For an inefficient measurement, the variance of the outcomes is larger, which represents uncertainty due to loss or noise. For unit efficiency, there is a residual variance due to vacuum fluctuations of the readout signal and overlap between the Gaussian distributions due to this effect leads to the measurement being nonprojective, or weak. The limit of projective measurement can be recovered by either letting $k \to \infty$, i.e., making the measurement infinitely strong, or $\Delta t \to \infty$, corresponding to an infinitely long measurement time. As noted earlier, putting the system initially into the equal superposition state ψ_0 and then measuring X can project the system into a maximally entangled state, but the probability for achieving this by measurement alone cannot exceed 50%. In the following sections we will see that feedback can increase this probability to 1.

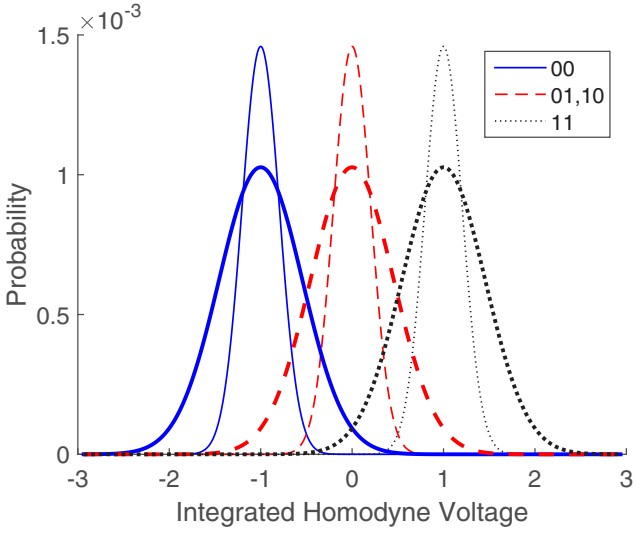

FIG. 1. (Color online) Histograms of the integrated measurement signal for the three eigenstates ρ_i of the measurement, given by $\mathrm{Tr}[\Omega_{\Delta V,\eta}\rho_i\Omega_{\Delta V,\eta}^\dagger]$. Plots are for $\eta = 1$ (thin lines) and $\eta = 0.2$ (thick lines) and use the parameters $\Delta t = 3\ \mu$s and $k = 1(2\pi)$ MHz.

III. OPTIMAL ROTATION IN A SINGLE TIME STEP

The only nonlocal resource in our deterministic entanglement scheme is the half-parity measurement X that was introduced in the previous section. Due to the lack of direct qubit-qubit coupling, the remaining control resource, the quantum feedback operations, will be restricted to local rotations that act on each qubit individually. Specifically, we define the feedback unitary as

$$U_F[\theta_1,\theta_2,\phi_1,\phi_2] = U(\theta_1,\phi_1) \otimes U(\theta_2,\phi_2), \quad (7)$$

where

$$U(\theta,\phi) \equiv \hat{I}_2 \cos\theta/2 - i\hat{\mathbf{n}}(\phi)\cdot\hat{\boldsymbol{\sigma}} \sin\theta/2$$

is a general single-qubit unitary rotation [$\hat{\boldsymbol{\sigma}}$ is a 3-vector of the Pauli matrices, $\hat{\mathbf{n}}(\phi)$ is a real 3-vector of unit norm, and $\hat{I}_2$ is the identity matrix]. Given the starting point of the equal superposition state $|\psi_0\rangle$, any target state lying within the triplet manifold may be obtained by rotations within a fixed ϕ plane of the Bloch sphere of each qubit. Hence we set $\hat{\mathbf{n}}(\phi)\cdot\hat{\boldsymbol{\sigma}} = \sigma_x\cos\phi + \sigma_y\sin\phi$. We note that in the presence of dephasing one might wish to remove this restriction and additionally allow σ_z rotations in order to introduce rotations between the target state $|t0\rangle \equiv \frac{1}{\sqrt{2}}(|01\rangle + |10\rangle)$ and the corresponding singlet $|s\rangle = \frac{1}{\sqrt{2}}(|01\rangle - |10\rangle)$. However, our measurement operator X is not capable of distinguishing these two states and so does not yield any direct information determining when to apply this operation. Hence the present construction of optimal strategies will assume negligible decoherence, although we retain the density-matrix element ρ_{ss} throughout the analysis in order to study the impact of dephasing (see Sec. VII).

Our goal is to find the optimal values of θ_i and ϕ_i as a function of time and measurement outcomes ΔV that will maximize entanglement. We choose the fidelity [38] of ρ with respect to the pure state $\rho_{t0} \equiv |t0\rangle\langle t0|$, i.e., $\mathcal{F}(\rho,\rho_{t0}) \equiv \mathrm{Tr}[\sqrt{\sqrt{\rho_{t0}}\rho\sqrt{\rho_{t0}}}]^2 = \rho_{t0t0}$, as a proxy for entanglement rather than the concurrence [39] with this state, since the former yields a figure of merit that is linear in the state ρ. We further simplify the setup by enforcing identical local feedback unitaries satisfying the properties $\theta_1 = \theta_2$ and $\phi_1 = \phi_2 = \pi/2$. The triplet subspace is closed under local unitary rotations satisfying these constraints. We assume that the initial state is in the triplet subspace, so we do not require the general rotations that connect the singlet and triplet subspaces. This is consistent with initializing in the equal superposition state $|\psi_0\rangle$.

In order to find the optimal feedback rotation after a measurement, regardless of whether this is in a

discrete- or infinitesimal-time increment, we parametrize the density matrix as follows:

$$\rho = \begin{bmatrix} \rho_{t-t-} & \rho_{t-t0} & \rho_{t-t+} & \rho_{t-s} \\ \rho^*_{t-t0} & \rho_{t0t0} & \rho_{t0t+} & \rho_{t0s} \\ \rho^*_{t-t+} & \rho^*_{t0t+} & \rho_{t+t+} & \rho_{t+s} \\ \rho^*_{t-s} & \rho^*_{t0s} & \rho^*_{t+s} & \rho_{ss} \end{bmatrix}, \quad \mathcal{F} = \rho_{t0t0},$$

where $|t-\rangle \equiv |00\rangle$, $|t+\rangle = |11\rangle$, and $|s\rangle \equiv \frac{1}{\sqrt{2}}(|01\rangle - |10\rangle)$. Since we are restricting the feedback operations to σ_y rotations ($\phi = \pi/2$) and our measurement is represented by a real matrix, we may further restrict ρ to be a real matrix. The fidelity with respect to $|t0\rangle$ after applying identical σ_y rotations on both qubits is given by

$$\begin{aligned} \mathcal{F}_1 &= \langle t0|\rho_1|t0\rangle \\ &= \mathcal{F} + \tfrac{1}{4}(\sqrt{8}\sin 2\theta(\rho_{t-t0} - \rho_{t0t+}) \\ &\quad + (1-\cos 2\theta)(1 - 3\mathcal{F} - 2\rho_{t-t+} - \rho_{ss}), \end{aligned} \tag{8}$$

where $\rho_1 = U_F[\theta,\theta,\frac{\pi}{2},\frac{\pi}{2}]\rho U_F^\dagger[\theta,\theta,\frac{\pi}{2},\frac{\pi}{2}]$. The optimal rotation angle θ is then found by maximizing $\langle t0|\rho_1|t0\rangle$ over θ and is given by

$$\begin{aligned} \theta_{\text{opt}}[\rho] = \tfrac{1}{2}\arctan[\sqrt{8}(\rho_{t-t0} - \rho_{t0t+}), 3\mathcal{F} \\ + \rho_{ss} + 2\rho_{t-t+} - 1], \end{aligned} \tag{9}$$

where $\arctan[y,x]$ behaves as $\arctan[y/x]$, but with θ chosen in the correct quadrant, i.e.,

$$\arctan[y,x] = \begin{cases} \arctan[y/x], & x > 0 \\ \arctan[y/x] + \pi, & y \geqslant 0,\ x < 0 \\ \arctan[y/x] - \pi, & y < 0,\ x < 0 \\ (y/|y|)\pi/2, & x = 0. \end{cases} \tag{10}$$

Average-sense local optimality

Equation (9) defines the optimal feedback as a function of the density matrix in a single time step. This relation will define a locally optimal protocol (sometimes referred to as a greedy strategy [40]), meaning that the controller maximizes the figure of merit at each time step.[1] However this may not be viable for practical applications. Although the controller does in principle have access to the density matrix at every time step, actually calculating $\rho(t)$, e.g., using Eq. (3) or (6), amounts to dynamical state estimation, which may be too computationally intensive to implement on the fly, i.e., in real time, and hence experimentally infeasible. Ideally, one would prefer to provide a protocol that does not require storing and manipulating the entire measurement record.

In order to obtain an experimentally feasible protocol, we drop the requirement that a protocol be locally optimal and instead search for one that is ASLO. To define such a protocol, we first define the average evolution over a single iteration of measurement and feedback to be the final state averaged over all measurement outcomes. Thus the average state $\bar{\rho}$ represents the state of knowledge of a controller that measures, applies feedback according to the measurement outcome, but then forgets which measurement outcome occurred and which feedback operation it applied. Average-sense locally optimal feedback is then given by the feedback operation that would be locally optimal if the average state were the actual state. This notion will allow us to define feedback protocols that can be applied with low computational overhead or even with a passive device. It also simplifies the analysis, since ASLO protocols are Markovian by definition.

Given an arbitrary feedback protocol $U_F[\rho]$, we define the average evolution over a time interval containing measurement and feedback by

$$\begin{aligned} \bar{\rho}(t+\Delta t) = \int U_F[\bar{\rho}_{\Delta V}(t+\Delta t)]\bar{\rho}_{\Delta V}(t+\Delta t) \\ \times U_F^\dagger[\bar{\rho}_{\Delta V}(t+\Delta t)]d(\Delta V) \end{aligned} \tag{11}$$

for discrete measurement and by

$$\begin{aligned} \bar{\rho}(t+dt) = \int U_F[\bar{\rho}_{dV}(t+dt)]\bar{\rho}_{dV}(t+dt) \\ \times U_F^\dagger[\bar{\rho}_{dV}(t+dt)]d(dV) \end{aligned} \tag{12}$$

for continuous measurement. In the sections that follow, we denote average quantities derived from $\bar{\rho}$, such as $\bar{\mathcal{F}}$ and $\bar{\theta}_{\text{opt}}$, by an overbar. Here $\bar{\rho}_{\Delta V(dV)}[t+\Delta t(dt)]$ is the state after a measurement initiated at time t, which is given by Eq. (6) [or Eq. (3)] acting on $\bar{\rho}(t)$ [but not yet performing the average over $\Delta V(dV)$]. Note that we are neglecting the time it takes to apply the unitary operations, so only the measurement contributes to the time duration of the feedback process. These equations represent the state update for the controller described above. Because we have set U_F to be a function of $\bar{\rho}_V$, we have implicitly restricted the feedback operation to depend only on the most recent measurement outcome $V(t)$ and the current time t, given the known time evolution of $\bar{\rho}(t)$. Consequently the feedback is Markovian. Furthermore, because of the integration over measurement outcomes, $\bar{\rho}(t)$ is *not* a stochastic quantity and thus one can solve Eq. (11) or (12) for $\bar{\rho}(t)$ given feedback protocol $U_F[\bar{\rho}_V]$ and initial state $\bar{\rho}(t=0)$.

The ASLO feedback operation $\bar{\theta}_{\text{opt}}$ is defined by replacing ρ with $\bar{\rho}_V$ in Eq. (9), which corresponds to applying the locally optimal feedback assuming that the actual state is $\bar{\rho}$. Because $\bar{\rho}$ is known from the outset, the ASLO feedback operation can be specified in a lookup table that can be computed beforehand for a given initial state. This is a substantial reduction in computational overhead and as we will see in later sections, this lookup table can in some instances be implemented by a passive device such as a mixer (multiplier), essentially making the feedback autonomous. In the following sections we will calculate the ASLO feedback strategy $U_F[V,t]$ for several cases and analyze their behavior for deterministic remote entanglement generation.

It is useful to analyze the symmetries of the framework that we have outlined above. Suppose we start in an initial state that is symmetric under the transformation $|0\rangle \leftrightarrow |1\rangle$ on both qubits (henceforth referred to simply as a 01-symmetric state). This symmetry implies that $\rho_{t+t+} = \rho_{t-t-}$, $\rho_{t-t0} = \rho_{t0t+}$, and $\langle X\rangle = 0$. Measurement can stochastically break this symmetry

[1] The term local refers to time local here and not spatially local (as in local unitary rotation).

by pushing the state toward $|00\rangle$ or $|11\rangle$. However, because the target state $|t0\rangle$ also respects this constraint, feedback will act equally and oppositely for these two cases [i.e., $\theta_{\rm opt}(V) = -\theta_{\rm opt}(-V)$] and thus this symmetry will be restored after integrating over V as in Eq. (11) or (12). Thus we may assume throughout that $\bar{\rho}$ retains 01 symmetry so long as the initial state does and thus $\bar{\rho}_{t+t+} = \bar{\rho}_{t-t-}$, $\bar{\rho}_{t-t0} = \bar{\rho}_{t0t+}$, and $\langle X\rangle_{\bar{\rho}} = 0$. Note that unlike both the target and equal superposition state, which are both 01 symmetric, the ground state $|11\rangle$ is an example of a state that is not 01 symmetric and thus we have excluded a natural initial state for the problem. However, in this case it is locally optimal to apply a $\pi/2$ rotation on both qubits, after which we will be in the equal superposition state $|\psi_0\rangle$.

While feedback strategies designed in this manner may not perform as well as those in which full dynamical state estimation is used at each time step, the added simplicity of average-sense local optimality makes the resulting protocols substantially simpler to implement experimentally. Note that until Sec. VI, none of the strategies we formulate attempt to surpass the performance of a locally optimal protocol.

IV. DISCRETE FEEDBACK AND THE SEMICLASSICAL PROTOCOL

We now consider specific feedback protocols based on ASLO introduced in the previous section. In this section we consider the situation where the quantum efficiency of the measurement is small, i.e., $\eta \ll 1$, which is a highly relevant scenario in many experimental settings. In this regime, measurement-induced dephasing quickly reduces the off-diagonal elements of the density matrix to zero [see Eq. (3)], so the controller only has access to the classical probabilities associated with the three measurement eigenstates. Without knowledge of the coherences, we arrive at a semiclassical protocol. This not only will provide a useful comparison to the more general quantum protocol derived in the following section, but will also be important for developing a hybrid protocol for arbitrary but not necessarily small efficiency $\eta < 1$ (Sec. VI).

In the limit of very small η, off-diagonal elements of $\bar{\rho}(t)$ will be approximately 0. To study feedback in this case, we explicitly set the off-diagonal elements to be some small quantities $\bar{\rho}_{t-t0} = \bar{\rho}_{t0t+} = \epsilon$ and $\bar{\rho}_{t-t+} = \epsilon'$, respectively, so that the first argument y of the arctan function in Eq. (9) and thus $\arctan[y/x]$ are approximately zero. If the second argument x is positive, i.e., $3\bar{\mathcal{F}}_{\Delta V} - 1 - 2\epsilon' \approx 3\bar{\mathcal{F}}_{\Delta V} - 1 > 0$, then $\bar{\theta}_{\rm opt} = 0$ (assuming for simplicity of the resulting equations that the singlet subspace is unpopulated). Using Eq. (6), we see that for an initially-01-symmetric state with fidelity $\bar{\mathcal{F}}$, the fidelity $\bar{\mathcal{F}}_{\Delta V}$ after measurement is given by

$$\bar{\mathcal{F}}_{\Delta V} = \frac{\bar{\mathcal{F}}}{\bar{\mathcal{F}} + \frac{1-\bar{\mathcal{F}}}{2}(e^{-4\eta k\Delta t(1+2\Delta V)})(1+e^{16\eta k\Delta t\Delta V})}. \quad (13)$$

Because Eq. (13) decreases monotonically away from $\Delta V = 0$, the above inequality yields a threshold behavior for the feedback strategy, in which the preferred operation is to do nothing unless $|\Delta V|$ exceeds some critical value $V_{T,\rm opt}$. In this case $x < 0$ and then $\bar{\theta}_{\rm opt} = \pm\pi/2$ where the sign is chosen to match the sign of y. Using Eq. (4) to calculate y, it is not difficult to show that the sign of y is the same as that of $\epsilon\Delta V$.[2] The optimal threshold voltage is given as

$$V_{T,\rm opt} = \frac{1}{8\eta k\Delta t}\operatorname{arccosh}\left[\frac{2\bar{\mathcal{F}}}{1-\bar{\mathcal{F}}}\exp(4\eta k\Delta t)\right], \quad (14)$$

which defines the semiclassical protocol. Note that $V_{T,\rm opt} = 1/2$ in the projective measurement limit $k\Delta t \gg 1$. Equation (14) has a simple interpretation. If the state is already entangled with high probability, the controller does nothing. If the probability of being in either $|t-\rangle$ or $|t+\rangle$ is above a certain threshold, one applies a $\pm\pi/2$ pulse to both qubits, which essentially resets the state to the product state $\frac{1}{2}(|0\rangle + |1\rangle) \otimes (|0\rangle + |1\rangle) = |\psi_0\rangle$ and gives the joint measurement another chance to collapse to the entangled $|t0\rangle$ state. Figure 2 shows the performance of this feedback strategy, in which fidelity is calculated according to Eq. (11).

This strategy is classical in the sense that the optimal feedback could just as easily be calculated by using the classical Bayes rule to combine prior state knowledge with the information gathered from the previous measurement to determine whether it is beneficial to apply feedback or do nothing [41]. Note that the larger $\bar{\mathcal{F}}$ is, the larger $V_{T,\rm opt}$ is and hence the wider the range of voltage in which no operation is performed, $[-V_{T,\rm opt}, V_{T,\rm opt}]$. Qualitatively, this is because as

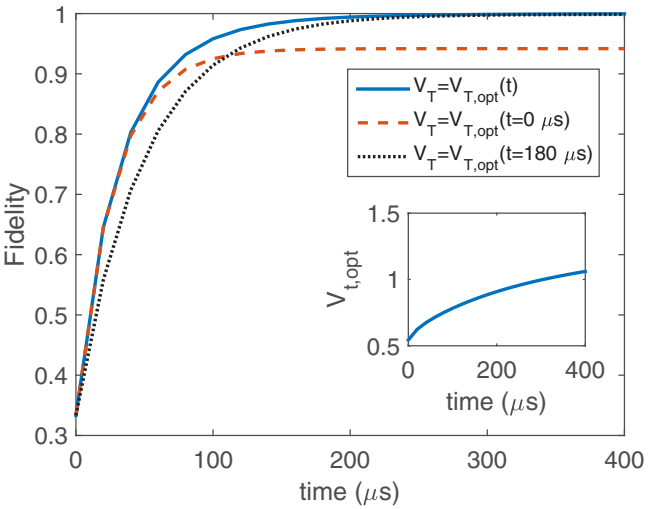

FIG. 2. (Color online) Discrete-time feedback simulations, showing fidelity with the $|t0\rangle$ state as a function of time, starting from the maximally mixed state in the triplet subspace. For these simulations, $\eta = 0.1$, $k = 1(2\pi)$ MHz, and $\Delta t = 20$ μs. The inset shows the optimal threshold voltage as a function of time. Note that for a smaller threshold, fidelity increases quickly at first but then saturates to a value significantly less than one, while for a larger constant threshold, fidelity increases slowly at first but then surpasses the former and approaches unity, though it does not asymptotically approach 1 [see Eq. (15)]. The locally optimal strategy, which increases the threshold as a function of time, matches or surpasses both fixed-threshold strategies at all times.

[2] If ϵ is identically zero, then one may take it to be an infinitesimal positive or negative value when calculating $\bar{\theta}_{\rm opt}$.

the fidelity with $|t0\rangle$ increases, it becomes more likely that the qubits are in the entangled state and so new information needs to suggest with higher probability that the system is in $|t-\rangle$ or $|t+\rangle$ before applying a rotation is beneficial, consistent with the Bayesian interpretation.

If one instead uses a fixed threshold value for feedback, one can analytically solve for the steady-state fidelity under this protocol:

$$\bar{\mathcal{F}}_{ss} = \langle t0|\bar{\rho}(\infty)|t0\rangle = 1 - \frac{4\,\mathrm{erfc}\left[\frac{V_T}{\sigma}\right]}{\mathrm{erfc}\left[\frac{(V_T+1)}{\sigma}\right] + 4\,\mathrm{erfc}\left[\frac{V_T}{\sigma}\right] + \mathrm{erfc}\left[\frac{(V_T-1)}{\sigma}\right]}, \quad (15)$$

where $\sigma \equiv 1/\sqrt{4k\eta\Delta t}$ is the standard deviation of the measurement operator and erfc is the complement error function $1 - \mathrm{erf}(x)$. We can see by taking limits of this expression that one can only reach unit steady-state fidelity in the limit that $V_T \gg \sigma$ or, in other words, the threshold voltage is much greater than the variance of the Gaussian weak measurement effect (5).

The discussion above defines a viable locally optimal discrete feedback protocol using a half-parity measurement. Feedback applied to a full-parity measurement has been used to deterministically entangle qubits located in the same cavity [26], without analysis or proof of any optimality properties. A different protocol was described in [42].

V. THE CONTINUOUS-TIME CASE AND QUANTUM PROTOCOL

If one attempts to derive a continuous-time protocol using the above result, the increase in fidelity becomes arbitrarily slow in the small-Δt limit. This is problematic for implementations. The underlying issue is apparent from examination of the $\Delta t \to 0$ limit if the threshold voltage in Eq. (14) is taken. Here $V_{\mathrm{T,opt}}$ diverges as $1/\Delta t$, but the standard deviation of the measurement outcomes diverges more slowly, as $1/\sqrt{\Delta t}$. (We note that the fact that these quantities diverge is an artifact of our normalization convention for ΔV. No physical observable diverges in this limit.) Thus the probability that this feedback strategy will result in performing any operation on the state vanishes. In order to derive a viable continuous-time protocol, we must therefore include coherences and take the full density matrix into account instead of just the diagonal elements.

We approach this by recognizing that Eq. (9) itself defines an ASLO protocol and can therefore be used to derive both discrete- and continuous-time feedback strategies directly, without setting the off-diagonal terms of ρ to zero. Figure 3 shows the performance of this discrete-time strategy in the case of perfect efficiency $\eta = 1$ for various choices of Δt and compares with the semiclassical protocol derived in the preceding section. Not surprisingly, Fig. 3 shows that the quantum protocol has a strictly better performance over the semiclassical protocol. However, the performance gap between the two protocols closes as Δt increases. The reason for this is that both the measurement-induced dephasing and the time interval between feedback operations increases as Δt increases, so the density matrix for which the feedback is calculated becomes closer and closer to a diagonal form. One can see this behavior explicitly in Fig. 3(b), in which

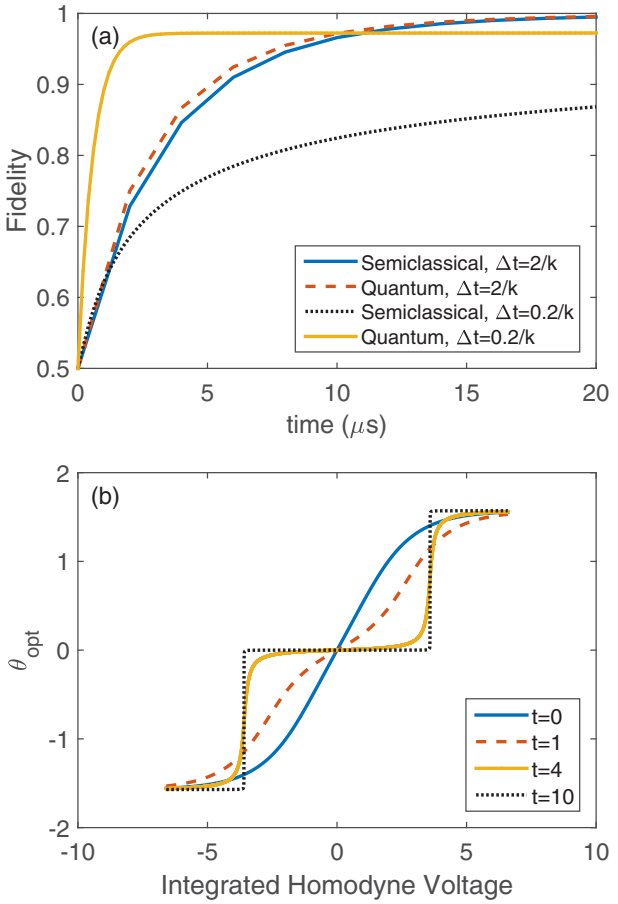

FIG. 3. (Color online) (a) Discrete feedback simulations, showing fidelity with the $|t0\rangle$ state as a function time under the semiclassical and quantum feedback [Eq. (9)] strategies, starting in the equal superposition state $|\psi_0\rangle$ and assuming a unit efficiency measurement and $k = 1(2\pi)$ MHz. The performance also changes according to the discrete time step Δt: we show two representative cases here. (b) Feedback $\theta_{\mathrm{opt}}(V)$ applied by the quantum protocol shown in (a) for the case $\Delta t = 0.2/k$ at four distinct time steps. At the latest time step, θ_{opt} resembles the semiclassical protocol because the off-diagonal elements of the density matrix have decayed to zero.

we plot the applied feedback as a function of the measurement outcome. At late times, it resembles the semiclassical protocol. We will revisit this point in Sec. VI.

The above example still constitutes discrete feedback, in which the measurement and feedback unitary rotations act sequentially. To derive a continuous protocol, we take the measurement strength to be small and assume that infinite strength rotations are available. We show below that this unphysical assumption will be unnecessary, but it is convenient for the initial derivation.

Given that $\bar{\rho}$ is 01 symmetric for any evolution starting from an initially-01-symmetric state, $dV \propto dW$ because $\langle X\rangle = 0$. Furthermore, inspection of Eq. (3) shows that the quantity $\bar{\rho}_{t-t0,dV} - \bar{\rho}_{t0t+,dV}$ appearing in the first argument of the arctan function in Eq. (9) is infinitesimal and proportional to dW. We can then substitute the continuous-time measurement update in Eq. (3) into Eq. (9) and expand in a Taylor series with respect to $\bar{\rho}_{t-t0,dV} - \bar{\rho}_{t0t+,dV} \propto dW$. Assuming that the

second argument in the arctan function is greater than zero,[3] this yields a proportional feedback strategy in which the feedback rotation is proportional to the measurement outcome dW via

$$\bar{\theta}_{\rm opt} = \frac{4\sqrt{k\eta}\bar{\rho}_{t-t0}}{3\bar{\mathcal{F}} + \bar{\rho}_{ss} + 2\bar{\rho}_{t-t+} - 1} dW \tag{16}$$

or equivalently

$$\bar{P}_{\rm opt}(t) \equiv \frac{\bar{\theta}_{\rm opt}}{dV} = \frac{8\sqrt{2}k\eta\bar{\rho}_{t-t0}}{3\bar{\mathcal{F}} + \bar{\rho}_{ss} + 2\bar{\rho}_{t-t+} - 1}. \tag{17}$$

This shows that the ASLO feedback is in fact direct feedback in the continuous-time limit, where the feedback rotation angle is directly proportional to the measurement value. This is the type of feedback is modeled by a Wiseman-Milburn feedback master equation [5,43] given in this instance by

$$d\bar{\rho}_V = \mathcal{D}[M]\bar{\rho}dt + \mathcal{H}[M]\bar{\rho}\sqrt{\eta}dW - i[H_F,\bar{\rho}]\frac{dW}{\sqrt{8\eta k}} - i[H_F,\{M,\bar{\rho}\}]\frac{dt}{\sqrt{8k}} + \mathcal{D}[H_F]\bar{\rho}\frac{dt}{8k\eta}, \tag{18}$$

with

$$H_F = \frac{\bar{P}_{\rm opt}(t)}{2}(\sigma_{y1} + \sigma_{y2}). \tag{19}$$

Here $d\bar{\rho}$ may be calculated as before using the averaged version of Eq. (18), i.e., integrating out dW. Substituting Eq. (17) into Eq. (18) then yields the equations of motion for the state under the ASLO quantum, continuous-time protocol. While this equation is difficult to solve in the general case, for $\eta = 1$ it admits an analytic solution when the initial state is pure and satisfies the usual symmetry property. To find this solution, we take the trial solution to be pure and 01 symmetric, so $\bar{\rho} = |\psi\rangle\langle\psi|$ with

$$|\psi(t)\rangle = \left[\sqrt{\frac{1-\bar{\mathcal{F}}(t)}{2}}, \sqrt{\bar{\mathcal{F}}(t)}, \sqrt{\frac{1-\bar{\mathcal{F}}(t)}{2}}, 0\right]^{\mathsf{T}}. \tag{20}$$

Substituting this form into Eq. (18) yields the following differential equation for $\bar{\mathcal{F}}$:

$$\frac{d\bar{\mathcal{F}}}{dt} = 2k(1-\bar{\mathcal{F}}) \Rightarrow \bar{\mathcal{F}}(t) = 1 - [1-\bar{\mathcal{F}}(0)]e^{-2kt}. \tag{21}$$

Crucially, the terms in Eq. (18) that depend on dW cancel upon substitution. This cancellation ensures that the actual state equals the average state at all times, i.e., $\bar{\rho}(t) = \rho(t)$, so the average state evolution is pure under this feedback protocol. This implies that the nonaveraged evolution is also deterministic and thus dynamical state estimation is not necessary to implement the locally optimal strategy in this special case.

[3]If we start in the separable state $(|0\rangle + |1\rangle) \otimes (|0\rangle + |1\rangle)$ as is most practical, this constraint will hold true for all later times. If we start in a state that does not satisfy this property, it is locally optimal to first apply a $\pi/2$ rotation on both qubits, after which the second argument will be greater than zero.

Having a solution for the evolution of the full density matrix in the case $\eta = 1$ also yields an analytic solution for the optimal proportionality coefficient between feedback and measurement $P_{\rm opt}$ as a function of time:

$$P_{\rm opt}(t) = \frac{4k[1-\mathcal{F}(0)]}{\sqrt{[1-\mathcal{F}(0)][\mathcal{F}(0) - 1 + e^{2kt}]}}. \tag{22}$$

This equation displays a marked similarity to the optimal feedback for single-qubit purification [9], with the functional form differing only by two minus signs in distinct locations. Like this quantum protocol for pure states, the single-qubit state evolution under optimal feedback is also deterministic and has been shown to be globally optimal for $\eta = 1$ [9,12,14]. These parallels lead us to speculate that the protocol given by Eq. (22) may be globally optimal as well. In the case of nonunit measurement efficiency, $\bar{\mathcal{F}}$ appears to exactly follow an exponential that asymptotically approaches a value less than 1. However, we have not been able to find an analytic solution.

Figure 4 shows the fidelity as a function of time using the quantum protocol for $\eta = 1$, comparing the performance of the ASLO protocol with time-dependent $P_{\rm opt}(t)$ (blue line) to that obtained by using a constant multiple of the zero time value $P_{\rm opt}(0)$ (red and yellow dotted lines). The superiority of the ASLO protocol is evident.

It is useful to study the asymptotic behavior of these protocols. The numerical simulations show that with the ASLO strategy, the fidelity quickly asymptotically approaches one, while using a constant multiple of $P_{\rm opt}(0)$ does not reach unit

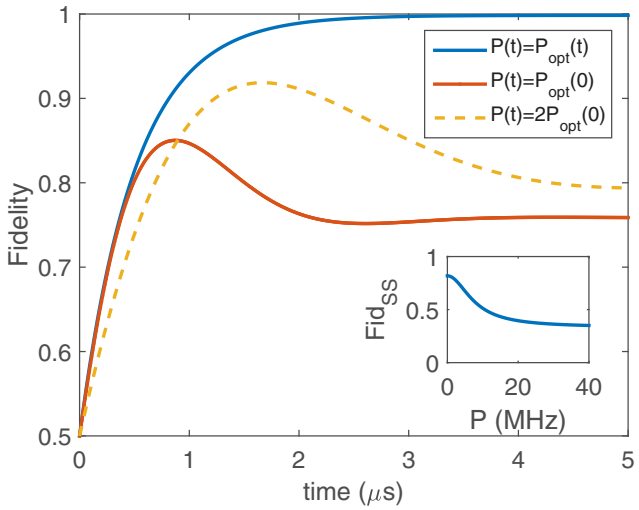

FIG. 4. (Color online) Continuous feedback simulations, showing fidelity with the $|t0\rangle$ state $\bar{\mathcal{F}}$ as a function of time under the continuous-time ASLO protocol given in Eq. (17). The initial state is the separable state $|\psi_0\rangle$. The simulation parameters are $k = 1(2\pi)$ MHz and $\eta = 1$, with time step $dt \ll 1/k$. Fidelity as a function of time for several values of constant proportionality coefficient P are also shown for comparison. The inset shows the steady-state fidelity $\bar{\mathcal{F}}_{ss,f}$ achieved for constant P, according to Eq. (23). Since we have taken the small dt limit, the threshold strategy would not change from its fidelity at $t = 0$. Note that if we were to plot the locally optimal strategy in this continuous-time situation, which would nomically require dynamical state estimation, it would coincide exactly with the curve for $P_{\rm opt}(t)$.

fidelity. This raises the question of whether a specific fixed value of P could also yield unit fidelity. By fixing $d\bar{\rho} = 0$ in Eq. (18), we obtain a system of linear equations that can be solved to yield the steady-state fidelity for fixed P:

$$\bar{\mathcal{F}}_{ss,f} = \frac{P^2 + 16k^2\eta(1+8\eta)}{3P^2 + 16k^2\eta(3+8\eta)}. \tag{23}$$

This result is valid for $P \neq 0$ (when $P = 0$, any state that commutes with the measurement is a steady state). For large P, the steady-state fidelity tends to $1/3$, while in the limit $P \to 0$, the steady-state fidelity is given by $(1+8\eta)/(3+8\eta)$. Moreover, since the denominator in Eq. (23) is greater than the numerator for all values of parameters, $\bar{\mathcal{F}}_{ss,f} < 1$. This analysis proves that it is not possible to obtain unit fidelity with a constant value of P and therefore a time-varying direct feedback protocol is necessary in order to reach unit fidelity at long times.

This quantum protocol has several appealing features for experimental realization. First, proportional feedback is realizable simply by using a mixer or analog multiplier [8], both of which have very low latency. Furthermore, unlike the semiclassical protocol, only infinitesimal rotations are called for in any given time step, which reduces the resources necessary for implementation.

VI. INEFFICIENT MEASUREMENT AND HYBRID PROTOCOLS

For unit efficiency, the fidelity quickly reaches 1 when continuous-time feedback is used. However, for $\eta < 1$, the fidelity asymptotically approaches a value less than 1 (see Fig. 5). Qualitatively, this happens because the off-diagonal elements of ρ that drive feedback in the continuous-time case [see Eq. (17)] decay faster relative to the feedback terms that increase the fidelity. In contrast, if we implement discrete-time feedback for the same value of $\eta < 1$, the fidelity increases more slowly at first, but eventually surpasses the asymptotic fidelity of the continuous-time strategy. Moreover, we know from Sec. IV that the semiclassical strategy is unaffected by decay of the off-diagonal terms and this strategy does reach a fidelity of 1. However, this strategy is only viable when the measurement time is finite. These facts suggest that we consider a hybrid protocol that transitions between continuous-time and discrete-time feedback, i.e., has a variable measurement duration.

To determine how to make this transition, we perform a numerical optimization of the measurement durations as follows. We divide the system evolution into 200 discrete steps each of duration Δt_i subject to the constraint $\sum_i \Delta t_i = T_{\text{final}}$. At each time step, discrete-time measurement, according to Eq. (5), followed by feedback according to the general optimal function (9) is applied. Then an optimization over all time intervals Δt_i is performed (using the gradient descent algorithm) to minimize the cost function $1 - \langle t0|\bar{\rho}(T_{\text{final}})|t0\rangle$.

The results of this optimization are shown in Fig. 5, where we plot the resulting fidelity as a function of time and compare to evolutions in which all Δt_i are fixed to a constant finite or an infinitesimal value. The optimization consistently finds a minimum in which the majority of the Δt_i intervals are small and approximately equal, while a few at the end are large. In other words, the optimal solution found by gradient descent shows a sharp transition between continuous-time feedback at short times to discrete-time feedback at long times. After the switching time, the off-diagonal elements are observed to be small and thus the applied feedback closely resembles that of the semiclassical protocol.

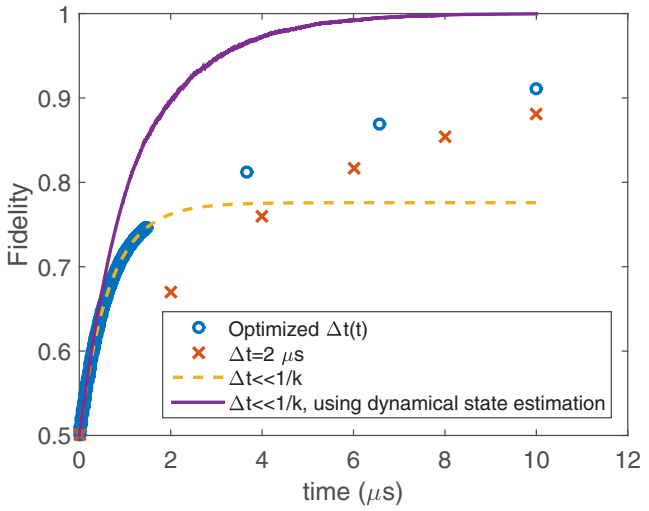

FIG. 5. (Color online) Fidelity $\bar{\mathcal{F}}$ starting from the $|\psi_0\rangle$ state as a function of time under the optimal variable-time-step protocol (blue circles), compared to fidelity obtained with constant-time-step protocols [discrete-time semiclassical protocol (red crosses) and continuous-time quantum protocol (yellow dotted line)]. The measurement is on continuously at a constant rate and feedback is applied instantaneously at each point in the graph. The parameters $k = 1(2\pi)$ MHz and $\eta = 0.4$ are chosen to illustrate the benefit of this optimized strategy for nonunit but not too small efficiency. The dense cluster of points before $t = 2$ μs shows that the gradient search resulted in almost all of the times for application of feedback to be located in the early stages of the evolution. Also shown is the fidelity obtained from a full non-Markovian strategy using dynamical state estimation and locally optimal feedback (see the text).

Since the measurement rate k is held constant in the above optimizations, an alternative way to view the change in optimal measurement time step is to view the finite duration measurements as a series of infinitesimal measurements. This perspective lends itself to the interpretation that when the hybrid protocol uses discrete feedback, it abstains from applying feedback at one time, only to apply a stronger feedback at a later time, and thus is not locally optimal. While we cannot prove any optimality properties of this hybrid protocol, its superior numerical performance indicates that it is significantly closer to global optimality than both of the fixed Δt protocols derived in previous sections.

Figure 5 also shows that there exists a non-Markovian strategy that outperforms the hybrid protocol described above. Simulating continuous feedback and averaging over 300 trajectories, we plot the fidelity as a function of time, assuming that the controller performs dynamical state estimation at each time step and then applies the optimal feedback unitary (9). Because simulation of trajectories tracks the actual state as opposed to the average state, this protocol is locally optimal, as opposed to ASLO. This strategy is found to surpass the hybrid

protocol at both early and late times, showing that for $\eta < 1$, dynamical state estimation can yield a better protocol than one based only on the average state. However, as discussed earlier (see Sec. III), such a non-Markovian protocol is generally more difficult to implement in practice.

VII. EXPERIMENTAL REALIZATION

In any experimental realization of the proposed feedback schemes to achieve entanglement between remote qubits, numerous imperfections will complicate the dynamics studied above. First, finite coherence of the qubits will limit the fidelity. Second, the above results apply only to truly Markovian dynamics, in which the controller acts instantaneously with an action that is based solely on the most recent measurement outcome. In practice, the homodyne measurement will have finite bandwidth and the feedback will necessarily act with some finite delay. In this section we present simulations of the continuous-time quantum feedback protocol specified in Eq. (17), in which these imperfections are now incorporated. We use the full stochastic master equation including finite detector bandwidth that is derived in [44],

$$d\rho = \mathcal{D}[M]\rho dt + \mathcal{H}[M]\rho\sqrt{\eta}dW + \mathcal{L}_{\rm q}dt - \frac{i}{\tau}[H_F,\rho] \times \int_{t_0}^{\infty} e^{-(s-t_0)/\tau}\left[2\langle X\rangle(t-s)ds + \frac{dW(t-s)}{\sqrt{\eta}}\right], \quad (24)$$

where $\mathcal{L}_{\rm q}$ models relaxation T_1 and dephasing T_ϕ on both qubits

$$\mathcal{L}_{\rm q} = \sum_i \left[\frac{1}{2T_{\phi,i}}\mathcal{D}[\sigma_{z,i}]\rho + \frac{1}{T_{1,i}}\mathcal{D}[\sigma_i]\rho\right]. \quad (25)$$

Notice that the term in large square brackets in Eq. (24) is simply dV. Simulations are for experimental parameters $\eta = 0.4$, dephasing times $T_{\phi,1} = 11.3\ \mu{\rm s}/2\pi$ and $T_{\phi,2} = 30\ \mu{\rm s}/2\pi$ for the first and second qubits, respectively, relaxation time $T_1 = 20\ \mu{\rm s}/2\pi$ [4], feedback delay $t_0 = 100$ ns, feedback loop bandwidth $1/\tau = 1.6(2\pi)$ MHz [8], and measurement rate $k = 1.3(2\pi)$ MHz. The effective dephasing times are obtained from combining an intrinsic qubit dephasing time of 30 $\mu{\rm s}/2\pi$ with a loss of 0.04 in amplitude units between the cavities due to the circulator, which amounts to an effective σ_z measurement on the first qubit by the environment [4].

To apply the average state feedback protocols, we assume that the effects of delay and finite bandwidth, the non-Markovian effects, are small, so that $\bar{P}_{\rm opt}(t)$ is unchanged after neglecting them. In this limit, we can then first run a simulation to calculate the average evolution $\bar{\rho}(t)$ using the continuous-time quantum protocol (12). This simulation incorporates decoherence but not the feedback delay or finite bandwidth effects. From this first simulation, we extract $\bar{P}_{\rm opt}(t)$ and we then apply this feedback coefficient to the stochastic simulations using Eq. (24), which are able to incorporate non-Markovian effects. This average performance is obtained here by averaging over 1500 stochastic trajectories. For these particular experimental parameters, dephasing prevents the fidelity from reaching the switching point observed above, which was confirmed by applying the same optimization as that of Sec. VI but including the above dephasing and decay rates. Therefore, in this case, our hybrid strategy dictates that we apply only continuous feedback.

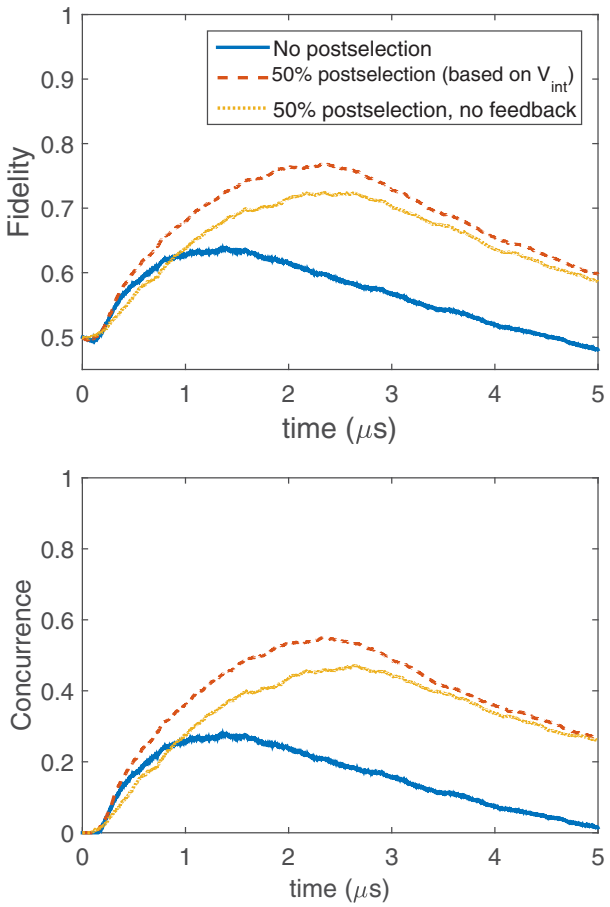

FIG. 6. (Color online) Continuous-feedback simulations, showing fidelity with the $|t0\rangle$ state as a function of time under the continuous-time ASLO protocol prescribed by Eq. (17) and incorporating experimentally realistic parameters and imperfections as described in the text. The fidelity reaches a much lower peak value than it would in the ideal case before decaying due to finite dephasing. Despite this, the fidelity substantially surpasses 50%, which is the threshold for entanglement. To directly quantify entanglement, we also plot the concurrence [45] as a function of time. Dashed and dotted curves show fidelity using a 50% postselection criterion with and without feedback, respectively.

Figure 6 shows the time dependence of the fidelity and concurrence resulting from this strategy, i.e., applying the continuous-time ASLO quantum feedback protocol in the presence of the additional experimental imperfections (solid blue lines). Figure 6 shows that existing technology is adequate to implement our proposal and to deterministically entangle two transmon qubits, since both the fidelity and concurrence achieved substantially surpass the corresponding entanglement thresholds to a significant degree. Although the average state feedback protocols derived here are motivated by the goal of achieving deterministic entanglement generation, one can also add postselection to this protocol even though, unlike the situation in measurement-induced entanglement without feedback [4], it is not essential here. The red dotted lines in Fig. 6 show the effect on the fidelity and concurrence of using

a 50% postselection, in which only the trajectories for which the absolute value of the integrated signal from 0 to 2.7 μs is less than the median are retained. The value of 2.7 μs was chosen to optimize the peak fidelity. This postselection method does not require any advanced processing of the signal and is seen to further enhance the fidelity and concurrence. We also plot the fidelity and concurrence using the same postselection criteria but without feedback, which confirms that feedback results in an improvement.

In the experiment of Ref. [8], the propagation through cables introduced the largest contribution to delay. Our results show that this delay has a measurable effect on the results of the simulation. It is conceivable that the delay could increase as the physical separation between the qubits is increased. It is useful to inquire whether our feedback protocol remains viable in this context. The answer to this question lies in the fact that the measurement strength k effectively sets the time scale for all feedback dynamics, as is evident in Eq. (18). Making the substitutions $k \to k/s$, $dt \to dts$, and $dW \to dW/\sqrt{s}$ leads to recovery of the same equation. Thus the effect of feedback delay and finite bandwidth can be removed simply by reducing the measurement strength. This has the effect of slowing down all the dynamics. Of course, one still encounters a limit set by the other absolute time scales inherent to the problem, in particular, the time scales for T_1 and T_2 processes. Nevertheless, this heuristic scaling argument shows that one can always choose k to strike a balance between delay and dephasing in order to optimize fidelity and that it is only the effective coherence times that will fundamentally limit the achievable entanglement.

In practice, increasing the distance between the qubits will also increase photon loss between cavities. Since the measurement probe has not yet interacted with the second qubit at this point, loss between cavities introduces additional dephasing on the first qubit. Such dephasing was seen to be significant in the experiment of Ref. [4], in which photon loss was dominated by the microwave circulator. Until better circulators are made, this source of loss is also likely to present a significant limitation to the maximum achievable entanglement using this scheme.

VIII. CONCLUSION

In this work we have developed several protocols for remote entanglement generation using measurement-based feedback that do not require real-time quantum state estimation. We introduced the notion of average-sense locally optimal protocols, in which the feedback operations are determined at a specific (local) time by maximizing the fidelity of the average state after a discrete or infinitesimal measurement with respect to the target state. Using this approach, we derived a quantum feedback scheme with local unitary operations that allows deterministic generation of entanglement when the measurements can be performed with unit efficiency ($\eta = 1$). The time local measurement averaging results in a Markovian feedback that is applicable to both discrete- and continuous-time implementation. In the continuous-time limit, the optimal ASLO quantum feedback becomes equivalent to simple proportional feedback, which is easily modeled using a Wiseman-Milburn equation [5,43] and may be realized in an autonomous fashion in experiments using a mixer (multiplier) [8]. The ASLO strategy was then used to develop a discrete-time step, semiclassical protocol, suitable for low measurement efficiencies and large time steps, in which only the classical probabilities for being in the entangled or unentangled states are taken into account. Analysis of the asymptotic behavior of both quantum and semiclassical protocols led to the development of a hybrid strategy that transitions from the quantum protocol at early times to the semiclassical strategy as the target state is approached at longer times, with an accompanying change in time step at the switching point. We demonstrated that such a hybrid strategy can be beneficial for the general case of intermediate measurement efficiency $\eta < 1$ with numerical optimizations and found strong evidence that the hybrid strategy is significantly closer to global optimality than any fixed-time-increment ASLO protocol.

The ASLO feedback strategies developed here possess interesting relationships to the locally optimal strategies for single-qubit purification by measurement and feedback [14]. In particular, the semiclassical protocol bears some resemblance to the locally optimal strategy for qubit purification in the small-η limit, while the quantum protocol at unit measurement efficiency also bears a striking resemblance to the corresponding optimal feedback for qubit purification in Ref. [14]. The advantages of combining two different strategies tailored to different measurement efficiencies in a single hybrid strategy were also observed in single-qubit purification, although here we have taken the additional step of optimizing the transition time.

We investigated the performance of these ASLO protocols for generation of remote entanglement between superconducting qubits with calculations based on existing superconducting 3D transmon technology. We found that even under the current conditions of relatively low measurement efficiency, the ASLO protocols can deterministically generate amounts of entanglement substantially surpassing the entanglement threshold [46]. In contrast, the known methods of heralded entanglement based only on measurements are always probabilistic. We further showed that in the presence of low measurement efficiency, one can also use postselection to further enhance the fidelity and we therefore developed a simple scheme based on the integrated signal to further enhance the fidelity to the target entangled state. This analysis highlights an interesting advantage of this remote entanglement generation scheme over others, such as those based on single-photon counting and the Hong-Ou-Mandel effect [47,48]. The ability to use feedback in our setup allows one to enhances the probability of success in a way that is not possible in these other heralded entanglement schemes. While the analysis presented in this work most immediately applies to superconducting qubits in microwave cavities, it could of course be adapted to any system in which one can implement a weak measurement of the half-parity observable defined in Sec. II.

This work suggests several future avenues for research that would be interesting from both a theoretical and an applied point of view. First, one could apply the verification theorems to address the question of whether or not our protocols are globally optimal [49]. In the case of unit efficiency and no decoherence, we speculate that our solution is globally optimal, although we have not attempted to prove

this statement. The deterministic evolution of the state under the quantum ASLO protocol indicates promise for this, in part because this feature, i.e., the deterministic evolution, is also observed in the globally optimal protocol for single-qubit purification. Second, while fidelity is a useful figure of merit for generating known states, concurrence may be more suitable for a detailed theoretical study and could yield additional insights. For instance, unlike fidelity, concurrence is invariant under the allowed feedback Hamiltonians, mirroring the behavior of entanglement. It would be useful to see whether this shared symmetry could be exploited. Finally, while we have ignored dephasing in the development of the ASLO feedback protocols, in applying the protocols to the realistic experimental setting for superconducting transom qubits, we found that dephasing presented the main limitation to performance. This suggests that it would be useful to investigate related protocols that would focus on correcting dephasing errors and hence assist with remote entanglement stabilization.

ACKNOWLEDGMENTS

We thank Mollie Schwartz and Irfan Siddiqi for many useful discussions. The work of L.M. was supported by the National Science Foundation Graduate Fellowship Grant No. 1106400 and the Berkeley Fellowship for Graduate Study. Sandia is a multiprogram laboratory managed and operated by Sandia Corporation, a wholly owned subsidiary of Lockheed Martin Corporation, for the United States Department of Energy's National Nuclear Security Administration under Contract No. DE-AC04-94AL8.

APPENDIX: DERIVATION OF FINITE-TIME POVM

As discussed in the main text, the stochastic master equation (SME) associated with a continuous-time QND measurement of the Hermitian observable X with strength k on a system with free Hamiltonian H is

$$d\rho = -i[H,\rho]dt + 2k\mathcal{D}[X]\rho dt + \sqrt{2k}\mathcal{H}[X]\rho dW(t). \quad \text{(A1)}$$

The superoperators $\mathcal{D}$ and $\mathcal{H}$ are defined in the main text. We assume that the measurement is unit efficiency and since it is QND, $[H,X] = 0$. This equation describes the evolution of the system conditioned on the measured voltage

$$dV(t) = \langle X\rangle(t)dt + \frac{dW(t)}{\sqrt{8k}}. \quad \text{(A2)}$$

The linear stochastic master equation [50–52] associated with this equation is

$$d\bar{\rho} = -i[H,\bar{\rho}]dt + 2k\mathcal{D}[X]\bar{\rho}dt + \sqrt{2k}\bar{\mathcal{H}}[X]\bar{\rho}dW(t), \quad \text{(A3)}$$

with $\bar{\mathcal{H}}[A]\bar{\rho} \equiv A\bar{\rho} + \bar{\rho}A^\dagger$. While Eq. (A1) is nonlinear in ρ and produces a normalized density matrix [i.e., $\mathrm{tr}(d\rho) = 0$], Eq. (A3) is linear in $\bar{\rho}$ and produces an unnormalized density matrix. Further, since this equation is linear we can restrict our focus to its action on pure states (since any density matrix is a convex sum of pure state density matrices). This defines the associated linear stochastic Schrödinger equation (SSE) [50]

$$d|\bar{\psi}\rangle = [(-iH - kX^2)dt + \sqrt{2k}dW(t)X]|\bar{\psi}\rangle. \quad \text{(A4)}$$

This is again a linear equation in the state $|\bar{\psi}\rangle$.

Both the linear SME and linear SSE sacrifice the normalization of the resulting state for linearity. To see what this means physically, note that both equations are consistent with $\langle X\rangle = 0$ and hence $dV(t) = \frac{dW(t)}{\sqrt{8k}}$, which means that we are generating conditional dynamics according to statistics associated with some fictitious (time-independent) state with property $\langle X\rangle = 0$. The real state $|\psi\rangle$ may not have this property and this is why the normalization is incorrectly predicted by Eq. (A4).

Despite this issue with unnormalized states, the utility of Eq. (A4) is that it is sometimes possible to analytically solve for $|\bar{\psi}\rangle$ (see, for example, Ref. [52]). In fact, the linear SSE in Eq. (A4) is in the easiest class of such equations to solve since all the operators in it commute. We are interested in the solution to Eq. (A4) over a small finite measurement time Δt. This can be solved explicitly and is given by [52])

$$\begin{aligned}|\bar{\psi}_{\Delta W}(t+\Delta t)\rangle &= e^{-iH\Delta t}e^{-2kX^2\Delta t+\sqrt{2k}X\Delta W}|\bar{\psi}(t)\rangle \\ &= e^{-iH\Delta t}e^{-2kX^2\Delta t+4kX\Delta V}|\bar{\psi}(t)\rangle \\ &\equiv \bar{\Omega}_{\Delta V}|\bar{\psi}(t)\rangle \end{aligned} \quad \text{(A5)}$$

for any initial state $|\bar{\psi}(t)\rangle$ (including normalized states), where $\Delta W = \int_t^{t+\Delta t} dW(t')$ is a Gaussian random variable. In the second line we have used the relation between the measured voltage and ΔW to write the solution in terms of the measured quantity ΔV, which has the probability distribution

$$P_{\Delta V} = \sqrt{\frac{4k}{\pi\Delta t}}e^{-\frac{4k\Delta V^2}{\Delta t}}. \quad \text{(A6)}$$

Equation (A5) generates states that do not quite yield correct predictions since the normalization of the state is incorrect. Consider a normalized initial state $|\psi(t)\rangle$. Then the probability of evolving during the measurement time according to the stochastic variation ΔV to time $t+\Delta t$ is not actually $\langle\bar{\psi}(t+\Delta t)|\bar{\psi}(t+\Delta t)\rangle$, but rather [50–52]

$$P_{\Delta V}\langle\bar{\psi}(t+\Delta t)|\bar{\psi}(t+\Delta t)\rangle = P_{\Delta V}\langle\psi(t)|\bar{\Omega}^\dagger_{\Delta V}\bar{\Omega}_{\Delta V}|\psi(t)\rangle.$$

This expression immediately tells us that the measurement operator associated with the true finite-time evolution is

$$\Omega_{\Delta V} = \sqrt{P_{\Delta V}}\bar{\Omega}_{\Delta V}, \quad \text{(A7)}$$

since the true probability of this stochastic evolution is $\langle\psi(t)|E_{\Delta V}|\psi(t)\rangle$ for the positive-valued effect $E_{\Delta V} = \Omega^\dagger_{\Delta V}\Omega_{\Delta V}$.

Now, solving for this effect for the QND measurement, we get

$$\begin{aligned}\Omega_{\Delta V} &= \left(\frac{4k}{\pi\Delta t}\right)^{\frac{1}{4}} e^{-iH\Delta t}e^{-\frac{2k\Delta V^2}{\Delta t}-2kX^2\Delta t+4kX\Delta V} \\ &= \left(\frac{4k}{\pi\Delta t}\right)^{\frac{1}{4}} e^{-iH\Delta t}e^{-2k\Delta t(\frac{\Delta V}{\Delta t}-X)^2}. \end{aligned} \quad \text{(A8)}$$

Here $\Omega_{\Delta V}$ is the finite-time measurement operator associated with the $\eta = 1$ weak QND measurement used in the main text (with $H = 0$) and $E_{\Delta V} = \Omega_{\Delta V}^\dagger \Omega_{\Delta V}$ is its corresponding effect.

For completeness we can also show that the effects defined above constitute a POVM since

$$\begin{aligned}
&\int_\infty^\infty d(\Delta V) dE_{\Delta V} \\
&= \int_\infty^\infty d(\Delta V) \Omega_{\Delta V}^\dagger \Omega_{\Delta V} \\
&= \int_\infty^\infty d(\Delta V) P_{\Delta V} e^{-4kX^2\Delta t + 8kX\Delta V} \\
&= \sqrt{\frac{4k}{\pi\Delta t}} e^{-4kX^2\Delta t} \int_\infty^\infty d(\Delta V) e^{-\frac{4k\Delta V^2}{\Delta t} + 8kX\Delta V} \\
&= \sqrt{\frac{4k}{\pi\Delta t}} e^{-4kX^2\Delta t} \sqrt{\frac{\pi\Delta t}{4k}} e^{4kX^2\Delta t} \\
&= \mathbf{1}. \qquad \text{(A9)}
\end{aligned}$$

Here the integral on the second line is a Gaussian integral that can be evaluated by completing the square in the exponent.

[1] H. J. Carmichael, *An Open Systems Approach to Quantum Optics* (Springer, Berlin, 1993).
[2] C. J. Hood, T. W. Lynn, A. C. Doherty, A. S. Parkins, and H. J. Kimble, Science **287**, 1447 (2000).
[3] K. W. Murch, S. J. Weber, C. Macklin, and I. Siddiqi, Nature (London) **502**, 211 (2013).
[4] N. Roch, M. E. Schwartz, F. Motzoi, C. Macklin, R. Vijay, A. W. Eddins, A. N. Korotkov, K. B. Whaley, M. Sarovar, and I. Siddiqi, Phys. Rev. Lett. **112**, 170501 (2014).
[5] H. M. Wiseman and G. J. Milburn, *Quantum Measurement and Control* (Cambridge University Press, Cambridge, 2009).
[6] J. E. Reiner, W. P. Smith, L. A. Orozco, H. M. Wiseman, and J. Gambetta, Phys. Rev. A **70**, 023819 (2004).
[7] C. Sayrin, I. Dotsenko, X. Zhou, B. Peaudecerf, T. Rybarczyk, S. Gleyzes, P. Rouchon, M. Mirrahimi, H. Amini, M. Brune *et al.*, Nature (London) **477**, 73 (2011).
[8] R. Vijay, C. Macklin, D. H. Slichter, S. J. Weber, K. W. Murch, R. Naik, and A. N. K. I. Siddiqi, Nature (London) **490**, 77 (2012).
[9] K. Jacobs, Phys. Rev. A **67**, 030301 (2003).
[10] H. M. Wiseman and J. F. Ralph, New J. Phys. **8**, 90 (2006).
[11] J. Combes and K. Jacobs, Phys. Rev. Lett. **96**, 010504 (2006).
[12] H. M. Wiseman and L. Bouten, Quantum Inf. Process. **7**, 71 (2008).
[13] J. Combes and H. M. Wiseman, J. Phys. B **44**, 154008 (2011).
[14] H. Li, A. Shabani, M. Sarovar, and K. B. Whaley, Phys. Rev. A **87**, 032334 (2013).
[15] C. Ahn, A. C. Doherty, and A. J. Landahl, Phys. Rev. A **65**, 042301 (2002).
[16] M. Sarovar, C. Ahn, K. Jacobs, and G. J. Milburn, Phys. Rev. A **69**, 052324 (2004).
[17] A. M. Brańczyk, P. E. M. F. Mendonça, A. G. Gilchrist, A. C. Doherty, and S. D. Bartlett, Phys. Rev. A **75**, 012329 (2007).
[18] H. M. Wiseman, Phys. Rev. Lett. **75**, 4587 (1995).
[19] R. L. Cook, P. J. Martin, and J. M. Geremia, Nature (London) **446**, 774 (2007).
[20] M. Sarovar and K. B. Whaley, Phys. Rev. A **76**, 052316 (2007).
[21] H. Mabuchi and P. Zoller, Phys. Rev. Lett. **76**, 3108 (1996).
[22] J. Wang and H. M. Wiseman, Phys. Rev. A **64**, 063810 (2001).
[23] D. A. Steck, K. Jacobs, H. Mabuchi, T. Bhattacharya, and S. Habib, Phys. Rev. Lett. **92**, 223004 (2004).
[24] J. K. Stockton, R. van Handel, and H. Mabuchi, Phys. Rev. A **70**, 022106 (2004).
[25] R. van Handel, J. K. Stockton, and H. Mabuchi, IEEE Trans. Autom. Control **50**, 768 (2005).
[26] D. Ristè, M. Dukalski, C. A. Watson, G. de Lange, M. J. Tiggelman, Y. M. Blanter, K. W. Lehnert, R. N. Schouten, and L. DiCarlo, Nature (London) **502**, 350 (2013).
[27] J. Wang, H. M. Wiseman, and G. J. Milburn, Phys. Rev. A **71**, 042309 (2005).
[28] M. Sarovar, H.-S. Goan, T. P. Spiller, and G. J. Milburn, Phys. Rev. A **72**, 062327 (2005).
[29] J. Kerckhoff, L. Bouten, A. Silberfarb, and H. Mabuchi, Phys. Rev. A **79**, 024305 (2009).
[30] Z. Liu, L. Kuang, K. Hu, L. Xu, S. Wei, L. Guo, and X.-Q. Li, Phys. Rev. A **82**, 032335 (2010).
[31] N. Nickerson, Y. Li, and S. Benjamin, Nat. Commun. **4**, 1756 (2013).
[32] M. A. Nielsen, Phys. Rev. Lett. **83**, 436 (1999).
[33] S. Lloyd and L. Viola, Phys. Rev. A **65**, 010101 (2001).
[34] F. Motzoi, K. B. Whaley, and M. Sarovar, Phys. Rev. A **92**, 032308 (2015).
[35] M. Silveri, E. Zalys-Geller, M. Hatridge, Z. Leghtas, M. Devoret, and S. Girvin, arXiv:1507.00732.
[36] K. Jacobs and D. A. Steck, Contemp. Phys. **47**, 279 (2006).
[37] K. Kraus, in *States, Effects, and Operations: Fundamental Notions of Quantum Theory*, edited by A. Böhm, J. D. Dollard, and W. H. Wootters, Lecture Notes in Physics, Vol. 190 (Springer, Berlin, 1983).
[38] R. Jozsa, J. Mod. Opt. **41**, 2315 (1994).
[39] W. K. Wootters, Phys. Rev. Lett. **80**, 2245 (1998).
[40] S. Dasgupta, C. Papadimitriou, and V. Umesh, *Algoritms* (McGraw-Hill, New York, 2008).
[41] A. N. Korotkov, arXiv:1111.4016.
[42] C. Hill and J. Ralph, Phys. Rev. A **77**, 014305 (2008).
[43] H. M. Wiseman, Phys. Rev. A **49**, 2133 (1994).
[44] H. Li, M. Sarovar, F. Motzoi, L. Martin, and K. B. Whaley (unpublished).
[45] S. Hill and W. K. Wootters, Phys. Rev. Lett. **78**, 5022 (1997).
[46] C. H. Bennett, G. Brassard, S. Popescu, B. Schumacher, J. A. Smolin, and W. K. Wootters, Phys. Rev. Lett. **76**, 722 (1996).
[47] J. Hofmann, M. Krug, N. Ortegel, L. Gérard, M. Weber, W. Rosenfeld, and H. Weinfurter, Science **337**, 72 (2012).
[48] H. Bernien, B. Hensen, W. Pfaff, G. Koolstra, M. Blok, L. Robledo, T. H. Taminiau, M. Markham, D. Twitchen, L. Childress *et al.*, Nature (London) **497**, 86 (2013).
[49] K. Jacobs and A. Shabani, Contemp. Phys. **49**, 435 (2008).
[50] P. Goetsch and R. Graham, Phys. Rev. A **50**, 5242 (1994).
[51] H. M. Wiseman, Quantum Semiclass. Opt. **8**, 205 (1996).
[52] K. Jacobs and P. L. Knight, Phys. Rev. A **57**, 2301 (1998).